Correlated-photon imaging with cancellation of object-induced aberration

D. S. Simon[1,2,*] and A. V. Sergienko[1,2,3]

[1]*Department of Electrical and Computer Engineering, Boston University, 8 Saint Mary's Street, Boston, Massachusetts 02215, USA*
[2]*Photonics Center, Boston University, 8 Saint Mary's Street, Boston, Massachusetts 02215, USA*
[3]*Department of Physics, Boston University, 590 Commonwealth Avenue, Boston, Massachusetts 02215, USA*
**Corresponding author: simond@bu.edu*

Received June 18, 2010; revised October 17, 2010; accepted November 12, 2010; posted November 17, 2010 (Doc. ID 130327); published January 10, 2011

We show that a recently discussed apparatus for aberration-canceled interferometry may be modified to perform correlated-photon imaging in the so-called "ghost" imaging configuration. For objects in the vicinity of a particular plane, the images are free of object-induced phase distortions. This apparatus has the distinctive feature that it may be used to superimpose images of two objects in a manner that could lead to useful effects and applications. We show that the apparatus works using either quantum-entangled or classically correlated light sources.

OCIS codes: 110.0110, 270.0270.

1. INTRODUCTION

Correlated-photon imaging, sometimes known as "ghost" imaging, was first discovered using entangled photon pairs [1] from spontaneous parametric downconversion (SPDC). It has since been found that most aspects of ghost imaging can be simulated using spatially correlated classical light [2,3], including thermal and speckle sources [4–9]. A separate line of research has shown that entangled photon pairs from downconversion may also be used to cancel some of the effects of frequency dispersion [10–12] or spatial dispersion (aberration) [13–15]. In [15], it was pointed out that it is possible to construct an interferometer such that if an object is placed in a particular plane, then the effects of all phase shifts induced by that object, including all object-induced aberrations, will cancel in the resulting coincidence rate. The goal here is to move away from interferometry and to produce an analogous effect in an imaging system. We show that this may be achieved by a simple variation of the traditional ghost imaging apparatus of Fig. 1. It is thus possible to produce images of the object's amplitude transmittance profile, undistorted by phase effects as long as the object is entirely contained within a small region near the special plane mentioned above. (For simplicity, we will only discuss transmission here; the case of reflection at the object is similar.) We then show that, although an entangled source was required for the temporal correlation experiments discussed in [13–15], a classical source with transverse spatial correlation will suffice for imaging.

In addition, if *two* objects are placed in the resulting optical system, one in each arm, the image produced will simply be the point-by-point product of the images that would be generated by each of the two separately. This is a new feature that does not appear if two objects are placed in the arms of other types of ghost imaging systems. We will comment on several possible applications of this effect below in Section 5.

We begin by briefly reviewing ghost imaging in Section 2, followed by a review of aberration-canceled interferometry in Section 3. We then show how a small change converts the aberration-canceled interferometer into a new type of ghost imaging system. We analyze this imaging system first with an entangled light source in Section 4, then with a classical source in Section 5. Finally, in Section 6 we discuss an important technical point about the need for lenses in front of the detectors, followed by conclusions in Section 7.

Microscopy of phase objects and the use of fluorescence-based methods are major areas of research in biological applications and currently tend to attract the most attention. However, the study of reflection and transmission microscopy of nonphase objects, such as the methods presented in the current paper, continue to be of interest. The applications of such methods in biomedical research alone are plentiful. To list just a few: imaging of collagen networks with reflection microscopy [16–19], reflection contrast microscopy (including the first successful localization of a specific gene on a human metaphase chromosome [20,21]), studies of optical propagation in artificial compound eyes [22], microspectroscopy and imaging of biomedical samples [23], and spatial mapping of the propagation of surface plasmon polaritons [24]. It is hoped that the methods given here may lead to enhancement of some of these applications.

2. CORRELATED-PHOTON IMAGING

Correlated-photon imaging or ghost imaging [1] is done with an apparatus like the one depicted schematically in Fig. 1. In the original version, the correlated-photon source is a $\chi^{(2)}$ nonlinear crystal pumped by a laser, leading to SPDC. Entangled photon pairs with anticorrelated momentum components $\mathbf{q}$ and $-\mathbf{q}$ transverse to the propagation direction travel along the two arms of the apparatus. The object to be viewed is placed in branch 2 (the upper branch), followed by a

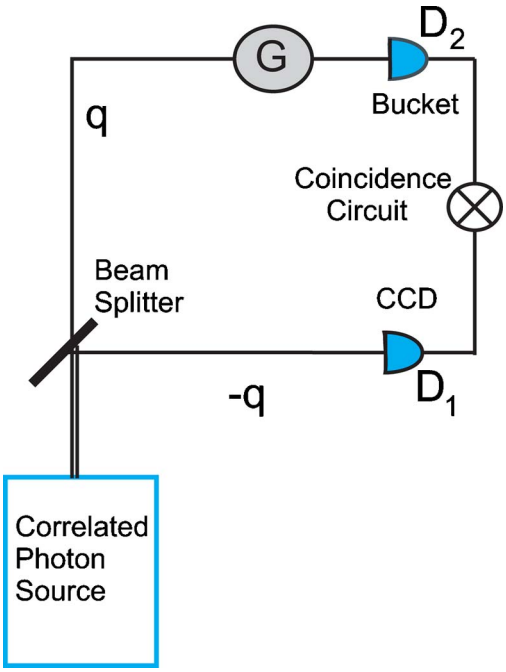

Fig. 1. (Color online) Schematic depiction of correlated-photon imaging setup. The photons in the two arms have anticorrelated transverse momenta $\pm\mathbf{q}$.

bucket detector, D_2. D_2 cannot record any information on the position or momentum of the photon that reached the object; it can only tell us whether or not the photon reached the detector unimpeded by an object. The other arm has no object, and all the photons reach a CCD camera or array of pointlike detectors without hindrance. A lens may be inserted in this branch for image formation. A coincidence circuit is used to record a count every time a photon detection occurs simultaneously (within a short time window) at each detector. By plotting the coincidence rate as a function of position $\mathbf{x}_1$ in detector 1, we build up an image of the object. This is true even though photons that actually encountered the object in branch 2 left no record of the object's position, and the photons in branch 1 that do carry position information never encounter the object.

The crucial ingredient is the spatial correlation of the photon pair. It was found [2,3] that entanglement was unnecessary: a classical source with anticorrelated transverse momenta could mimic the effect. The correlated light source in this case consists of a beam steering modulator (a rotating mirror, for example) directing a classical light beam through a range of $\mathbf{q}$ vectors, illuminating different spots on the object. The beam splitter turns the single beam of transverse momentum $\mathbf{q}$ into a pair of beams with momenta $\mathbf{q}$ and $-\mathbf{q}$. The results were similar to those with the entangled source, but with half the visibility. It was later shown that thermal and speckle sources may also lead to ghost imaging [4–9].

3. SUMMARY OF ABERRATION CANCELLATION IN QUANTUM INTERFEROMETRY

Consider the setup shown in Fig. 2 [13–15]. Each branch contains a $4f$ imaging system with lenses of focal length f and a thin object that provides spatial modulation $G_j(\mathbf{y})$ of the beam, where $j = 1, 2$ labels the branch and $\mathbf{y}$ is the position in the plane transverse to the axis. The goal is to cancel object-induced optical aberrations (position-dependent phase shifts produced by the G_j). The case of a single object in one branch only may be included by simply setting $G = 1$ in the other branch. The plane of the samples (labeled Π in Fig. 2) is the Fourier plane of the $4f$ system. Time delay τ is inserted in one branch. In the detection stage, two large bucket detectors D_1 and D_2, connected in coincidence, record the arrival of photons, but not their positions. Apertures described by pupil functions $p_1(\mathbf{x}_1)$ and $p_2(\mathbf{x}_2)$ are followed by crossed polarizers at 45° to each beam's polarization before arriving at the detectors.

A continuous wave laser pumps a $\chi^{(2)}$ nonlinear crystal, leading to collinear type II parametric downconversion. The frequencies of the two photons are $\Omega_0 \pm \nu$, with transverse momenta $\pm\mathbf{q}$. For simplicity, assume the frequency bandwidth is narrow compared to Ω_0. The two photons have total wavenumbers $\frac{\Omega_0 \pm \nu}{c} \approx \frac{\Omega_0}{c}$. The downconversion spectrum is

$$\Phi(\mathbf{q},\nu) = \mathrm{sinc}\left[\frac{L\Delta(\mathbf{q},\nu)}{2}\right] e^{\frac{iL\Delta(\mathbf{q},\nu)}{2}}, \tag{1}$$

where L is the thickness of the crystal, and

$$\Delta(\mathbf{q},\nu) = -\nu D + M\hat{\mathbf{e}}_2 \cdot \mathbf{q} + \frac{2|\mathbf{q}|^2}{k_{\mathrm{pump}}}. \tag{2}$$

D is the difference between the inverse group velocities of the ordinary and extraordinary waves in the crystal, and M is the spatial walk-off in the direction $\hat{\mathbf{e}}_2$ perpendicular to the interferometer plane. The last term in Δ is due to diffraction in the crystal. Ignoring the vacuum term and terms of higher photon number, the wave function entering the apparatus is approximately given by

$$|\Psi\rangle = \int \mathrm{d}^2 q\, d\nu \Phi(\mathbf{q},\nu) \times \hat{a}_s^\dagger(\mathbf{q},\Omega_0+\nu)\hat{a}_i^\dagger(-\mathbf{q},\Omega_0-\nu)|0\rangle, \tag{3}$$

where $\hat{a}_s$ and $\hat{a}_i$ are annihilation operators for the signal and idler photons. For collinear pairs, horizontally polarized photons are directed into the upper branch and vertically polarized photons are directed into the lower branch by means of a polarizing beam splitter. Alternatively, noncollinear pairs could be used with polarizers selecting horizontal (H) polarization in the upper branch and vertical (V) in the lower one.

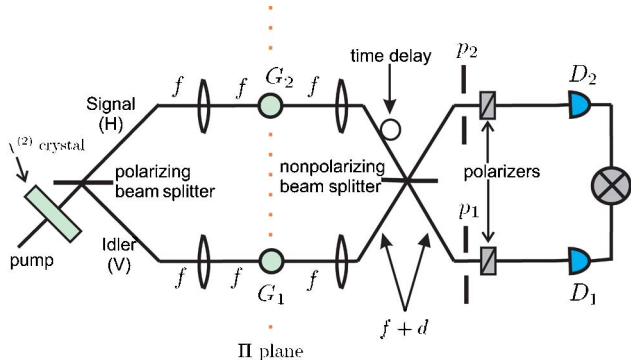

Fig. 2. (Color online) Schematic of interferometer with even-order aberration cancellation. Large bucket detectors D_1 and D_2 are integrated over and connected by a coincidence circuit.

In either case, we will refer to the H photon in the upper branch (branch 2) as the signal and the V photon in branch 1 as the idler.

The coincidence rate is of the generic form [25]

$$R(\tau) = R_0\left[1 - \Lambda\left(1 - \frac{2\tau}{DL}\right)W(\tau)\right], \tag{4}$$

where $\Lambda(x)$ is the triangular function:

$$\Lambda(x) = \begin{cases} 1 - |x|, & |x| \le 1 \\ 0, & |x| > 1 \end{cases}. \tag{5}$$

For large apertures, $p_1(\mathbf{x}_1) = p_2(\mathbf{x}_2) \approx 1$, so, as shown in [14], the background and τ-modulation terms are

$$R_0 = \int \mathrm{d}^2 q \left| G_1\left(\frac{f\mathbf{q}}{k}\right) G_2\left(-\frac{f\mathbf{q}}{k}\right)\right|^2, \tag{6}$$

$$W(\tau) = \frac{1}{R_0}\int \mathrm{d}^2 q e^{-\frac{2iM\tau}{D}}\mathbf{e}_2 \cdot \mathbf{q} \times G_1^*\left(\frac{f\mathbf{q}}{k}\right) G_1\left(-\frac{f\mathbf{q}}{k}\right) \times G_2^*\left(-\frac{f\mathbf{q}}{k}\right) G_2\left(\frac{f\mathbf{q}}{k}\right), \tag{7}$$

where k is the longitudinal wavenumber.

We may write $G_j(\mathbf{x}) = t_j(\mathbf{x})e^{i\phi_j(\mathbf{x})}$, with t_j real. Aberration effects arise from spatially dependent phase factors $\phi_j(\mathbf{x})$, which lead to distortion of the outgoing wavefronts. The phase functions may be decomposed into a sum of pieces that are either even under reflection, $\phi_j^{(\mathrm{even})}(-\mathbf{x}) = \phi_j^{(\mathrm{even})}(\mathbf{x})$, or odd, $\phi_j^{(\mathrm{odd})}(-\mathbf{x}) = -\phi_j^{(\mathrm{odd})}(\mathbf{x})$. Astigmatism and spherical aberration, for example, are included in the even-order part, whereas coma is odd.

In Eq. (7), the factors $G_1^*(\frac{f\mathbf{q}}{k})G_1(-\frac{f\mathbf{q}}{k})$ become

$$t_1^*\left(\frac{f\mathbf{q}}{k}\right) t_1\left(-\frac{f\mathbf{q}}{k}\right) e^{-i\left[\left(\phi_1\frac{f\mathbf{q}}{k}\right) - \phi_1\left(-\frac{f\mathbf{q}}{k}\right)\right]}. \tag{8}$$

The form of the difference in the exponent shows that even-order aberrations arising from object 1 cancel from the modulation term. The even-order aberrations from object 2 cancel in a similar manner. This is the even-order cancellation effect demonstrated in [13,14]. As pointed out in [15], even- and odd-orders cancel simultaneously only in the special case $G_1 = G_2$. These cancellations are exact only for aberrations induced by thin objects in the particular plane Π.

In the term R_0, both even-order and odd-order aberrations cancel even for $G_1 \neq G_2$. For time correlation experiments, this is an unimportant background term; however, this term is the foundation of the imaging apparatus described in Section 4, since the beam splitter will be absent, meaning that there will be no modulation term $W(\tau)$. The physical mechanism of the various possible cancellations are discussed in more detail in [15].

4. ABERRATION-CANCELLED GHOST IMAGING WITH ENTANGLED SOURCE

Now we wish to look at the ghost imaging analog of the aberration-canceling interferometer of Section 3. This leads us to the hybrid device of Fig. 3. This new apparatus differs from that of Fig. 2 in several respects. First, we have removed the time delay, polarization filters, and beam splitter; these were needed to produce the interference effects desired in [13–15] but are not necessary for imaging purposes. Also, in order to obtain spatial resolution, one bucket detector (D_1) is replaced by a moveable pointlike detector or a CCD camera. The removal of the beam splitter and the introduction of spatial resolution are the key changes. After allowing for an arbitrary source of correlated (quantum or classical) light, we arrive at an apparatus in Fig. 3 that looks very much like the ghost imaging setup of Fig. 1 but with a $4f$ imaging system in each branch. In this section, we assume that the light source is parametric downconversion.

The coincidence rate at location $\mathbf{x}_1$ of D_1 is

$$R(\mathbf{x}_1) = \int \mathrm{d}^2 x_2 dt_1 dt_2 |A(\mathbf{x}_1, \mathbf{x}_2, t_1, t_2)|^2, \tag{9}$$

where the transition amplitude is

$$A(\mathbf{x}_1, \mathbf{x}_2, t_1, t_2) = \langle 0|E_1^{(+)}(\mathbf{x}_1, t_1)E_2^{(+)}(\mathbf{x}_2, t_2)|\Psi\rangle. \tag{10}$$

Taking the two detection apertures described by p_1 and p_2 to be large, we compute the coincidence rate to be

$$R(\mathbf{x}_1) = \{[B(\mathbf{x}_1) + B(-\mathbf{x}_1)] + [C(\mathbf{x}_1) + C^*(\mathbf{x}_1)]\} \times \left|G_1\left(\frac{f}{f_D}\mathbf{x}_1\right) G_2\left(-\frac{f}{f_D}\mathbf{x}_1\right)\right|^2, \tag{11}$$

where

$$B(\mathbf{x}_1) = \int \mathrm{d}\nu \left|\Phi\left(\frac{k\mathbf{x}_1}{f_D}, \nu\right)\right|^2, \tag{12}$$

$$C(\mathbf{x}_1) = \int \mathrm{d}\nu \Phi\left(\frac{k\mathbf{x}_1}{f_D}, \nu\right)\Phi^*\left(-\frac{k\mathbf{x}_1}{f_D}, -\nu\right). \tag{13}$$

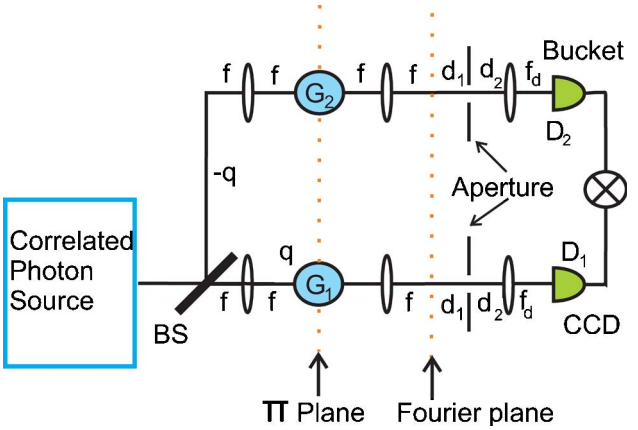

Fig. 3. (Color online) Schematic of correlated-photon imaging setup with aberration cancellation. All orders of aberration cancel.

Using Eq. (1), these integrals may be evaluated; they turn out to be x_1-independent constants. Sweeping all overall constants into a single constant $\mathcal{R}_0$, we find

$$R(\mathbf{x}_1) = \mathcal{R}_0 \left| G_1\left(\frac{f}{f_D}\mathbf{x}_1\right) G_2\left(-\frac{f}{f_D}\mathbf{x}_1\right)\right|^2. \tag{14}$$

Only the modulus of each G_j enters into $R(\mathbf{x})$, so we see that the aberrations introduced by the object phases cancel to all orders. This will be exact only in the Fourier plane, but as was true for the interferometer case, we would expect it to continue to remain approximately true as we move out of the plane up to a maximum distance of the order of $\frac{f r_s}{a}$, where f and a are the focal length and radius of the lens, and r_s is the maximum radius of the object being viewed. (See [15] for a derivation of this estimate.)

If $G_2 = 1$, then we have an ordinary (nonghost) image of $|G_1|$. On the other hand, if $G_1 = 1$ then we have an inverted ghost image of $|G_2|$. In either case, the image is magnified by a factor of $m = \frac{f_D}{f}$. Note that, in contrast to the interferometry case, even and odd-order phases both cancel, even in the general case $G_1 \neq G_2$. The cancellation of the phases only occurs in the Fourier plane; aberrative distortions begin growing when the objects are moved out of this plane.

In passing, note that d_1 and d_2 enter only into the coincidence amplitude's phase [which cancels due to the absolute square in Eq. (14)] and into the overall constants out front (which are absorbed into the normalization $\mathcal{R}_0$ of the counting rate). Therefore, d_1 and d_2 are unconstrained as long as the conditions of the derivation hold (i.e., that the object is confined to the plane Π and that all apertures are large).

5. APPLICATIONS TO IMAGE ANALYSIS

Note that if both G_1 and G_2 are nontrivial objects, what we actually see is their pointwise product. This is a distinctive feature of this apparatus. It can be verified by straightforward calculation that the simple product structure of Eq. (14) does not occur in other obvious variations of two-object ghost imaging systems; for example, it does not occur if the $4f$ imaging system in either branch (or both) is replaced by a single lens imaging system or by a system without lenses. We may make use of this product structure in a number of ways. For example, if G_2 has a dim, low-transmissivity area that we wish to view, but it is being obscured by a bright, high-transmissivity area nearby, we may use a mask for G_1 which allows a view only of the twins of photons coming from the dim region of interest, blocking photons that are partnered with light from other areas.

Alternatively, if the object of interest is G_2 but the second branch introduces some *known* distortion to its image, then this can be canceled by using an object G_1 that introduces an opposite distortion (via a deformable mirror, for example). The two distortions then cancel, leaving no net effect on the image. Consider two examples. (i) Suppose that a material with known distorting effect (a thin layer of some material or a microscope cover slip) is slightly *outside* the focal plane, in the path of the light. Equation (14) was derived for one specific plane; as the material moves away from that plane, the distorting phases no longer cancel. However, the product structure $G_1 \cdot G_2$ is still present, allowing for cancellation of the distortion by using a compensating object in the other branch. (ii) Similarly, Eq. (14) assumes that the lens apertures are large. As the lenses become smaller, Eq. (14) again becomes altered so that the phase cancellation is not complete. But the product structure may be used as before to provide corrections for this.

At first glance, the product structure might seem to open up a further interesting possibility. Suppose G_1 is the object we wish to view. If there is no object in branch 2 (G_2 is simply a constant), then the resolution with which we may view G_1 is the same as if the second branch was not there. It would be limited by the sizes of the Airy disks produced by the lenses. However, if G_2 is taken to be a small pinhole, the area we would be able to see of G_1 at any given time would be limited by the size of the pinhole. Thus, it would seem that, by making the pinhole small enough, we would be able to limit our view of G_1 to an area smaller than the standard Abbé limit, thus achieving subresolution imaging. Unfortunately, when the finite sizes of the lenses are properly taken into account [Eq. (14) was derived in the limit of large lenses], the combined action of diffraction in the two branches conspires to give the single-branch resolution as its best-case limit, occurring when the pinhole radius is negligible. As the pinhole radius at G_2 grows to finite size, the resolution becomes worse than in the single-branch case.

One additional observation on applications of the product structure arises if we replace the position-resolving detector in branch 1 by a bucket detector, thus introducing an integration over $\mathbf{x}_1$. We have now lost all imaging ability, but note what happens if we displace one of the objects (object 1, say) by some distance in the transverse plane. If the two-dimensional displacement vector is $\mathbf{r}$, then Eq. (14) is replaced by

$$R(\mathbf{r}) = \mathcal{R}_0 \int \left| G_1\left(\frac{f}{f_D}(\mathbf{x}_1 + \mathbf{r})\right) G_2\left(-\frac{f}{f_D}\mathbf{x}_1\right)\right|^2 \mathrm{d}x_1. \tag{15}$$

Thus, despite the fact that neither detector has spatial resolution, the system optically computes the spatial intensity correlator $g(\mathbf{r}) = \langle I_1(m^{-1}(\mathbf{x}+\mathbf{r}))I_2(-m^{-1}\mathbf{x})\rangle$, where m is the magnification. [The correlation here is actually between the object $G_1(\mathbf{x})$ and the *inverted* object $G_2(-\mathbf{x})$, but an additional lens can be added to remove the inversion and cancel the minus sign in G_2]. The full correlation function can be found by moving one object repeatedly to scan over the full range of relevant $\mathbf{r}$ vectors. Taking one of the two objects to be unknown and the other to be some known template, this could provide a means of identifying the unknown object by quantifying its degree of similarity to the template. This could be useful, for example, in comparing silicon chips on an assembly line to a standard chip and identifying those chips with flaws. Note in particular that the unknown object may be in a remote, inaccessible location; for example, the object might be a cell inside the body being viewed through an endoscope and compared to a cell in the lab. As in the case of the temporal correlator studied with the interferometer of [13–15], the effect of object-induced aberrations (differences between phase shifts induced by the two samples) cancels out of the spatial correlator.

6. IMAGING WITH A CLASSICAL SOURCE

We now replace the downconversion source of the previous section by a classical source of anticorrelated photons, as in [2]. Light entering a beam splitter with transverse momentum $\mathbf{q}$ leads to outgoing beams with anticorrelated momenta $\mathbf{q}$ and $-\mathbf{q}$. If the beam steering modulator produces momentum spectrum $f(\mathbf{q})$, the input state for pairs of photons having the same $\mathbf{q}$ before the beam splitter will be $\sim \int \mathrm{d}^2 q F(\mathbf{q}) \hat{a}_p^\dagger(\mathbf{q}) \hat{a}_p^\dagger(\mathbf{q})|0\rangle$, where $\hat{a}_p^\dagger$ is the creation operator for pump photons and $F(\mathbf{q}) \equiv f^2(\mathbf{q})$. We assume for simplicity that $F(\mathbf{q})$ is an even function, and $F(\mathbf{q}) = F(-\mathbf{q})$. Denoting creation operators in the two outgoing branches by $\hat{a}_1^\dagger$ and $\hat{a}_2^\dagger$, the incoming photon pair will produce a state after the beam splitter given by

$$|\Psi\rangle = \frac{1}{2}\int \mathrm{d}^2 q F(\mathbf{q})[\hat{a}_1^\dagger(\mathbf{q}) + \hat{a}_2^\dagger(-\mathbf{q})] \times [\hat{a}_1^\dagger(\mathbf{q}) + \hat{a}_2^\dagger(-\mathbf{q})]|0\rangle \quad (16)$$

$$= \int \mathrm{d}^2 q F(\mathbf{q})[\hat{a}_1^\dagger(\mathbf{q})\hat{a}_2^\dagger(-\mathbf{q}) + \ldots]|0\rangle, \quad (17)$$

where the terms dropped in the last line are those which do not contribute to coincidence detection. The detection amplitude of Eq. (10) is then proportional to

$$\int \mathrm{d}^2 q F(\mathbf{q}) e^{i\mathbf{q}\cdot(\mathbf{x}_1 - \mathbf{x}_2)} H_1(\mathbf{q}, \mathbf{x}_1) H_2(-\mathbf{q}, \mathbf{x}_2), \quad (18)$$

where H_j is the transfer function for branch j. Integrating over D_2, we then have the coincidence rate:

$$R(\mathbf{x}_1) = \left| F\left(\frac{k}{f_D}\mathbf{x}_1\right) G_1\left(\frac{f}{f_D}\mathbf{x}_1\right) G_2\left(-\frac{f}{f_D}\mathbf{x}_1\right)\right|^2. \quad (19)$$

This is similar to the result for the entangled-source apparatus, except modulated by the factor $F(\frac{k}{f_D}\mathbf{x}_1)$, which is determined by the details of the beam steering modulator. Similarly, for thermal or speckle sources, this factor will arise from the transverse momentum spectrum of the source.

Note that the form of the modulation factor can be controlled in a number of ways: for example, by using a spatial light modulator to manipulate the form of the incoming light, thus arranging a desired momentum distribution $F(\mathbf{q})$. Although we will not pursue the possibility further here, it is easy to imagine situations where the use of such controlled modulation might be advantageous. For example, it could facilitate the use of structured illumination in microscopy.

7. ROLE OF THE DETECTION LENS

Consider now the lenses immediately before the detectors in Fig. 3. With no such detection lens present, the transfer function for branch j would be

$$H_j(\mathbf{q}_j, \mathbf{x}_j) = G_j\left(\frac{f\mathbf{q}_j}{k}\right) e^{i\mathbf{q}\cdot\mathbf{x}_j}, \quad (20)$$

from which we see that the information from each $\mathbf{q}$ value is spread over all $\mathbf{x}$ values. But *with* the lens, Eq. (20) becomes

$$H_j(\mathbf{q}_j, \mathbf{x}_j) = e^{-\frac{ikx_j^2}{2f_D}\left(\frac{d_2}{f_D}-1\right)} e^{-\frac{id_1 q_j^2}{2k}} \times G_j\left(\frac{f\mathbf{q}_j}{k}\right)\delta\left(\frac{k\mathbf{x}_j}{f_D} - \mathbf{q}_j\right), \quad (21)$$

so that each $\mathbf{q}$ value is localized at a single point in the detector plane via the delta function. Since each $\mathbf{q}$ value is also matched to an object point, the localization in the second case defines a mapping between points in the object plane and points in the detection plane, allowing reconstruction of an image by the pointlike detector D_1. This can be verified by computing the coincidence rate with or without the final lenses, i.e., using either Eq. (20) or Eq. (21). Doing so, we find that, without the branch 1 lens, the coincidence rate becomes independent of $\mathbf{x}_1$, making imaging impossible. In contrast, removing the branch 2 lens has no effect. This makes intuitive sense: we integrate over $\mathbf{x}_2$, so it does not matter if the momentum information in this branch is localized or spread over the entire detector. Thus, we arrive at an important technical point: the lens before the bucket detector may be removed without harm, but the branch 1 lens is essential for imaging.

The need for a lens before D_1 may be viewed as follows. The $4f$ system in either branch transfers modulation G_j from the transverse coordinate space ($\mathbf{x}$) to the Fourier space ($\mathbf{q}$), which is where the aberration cancellation actually takes place (see [15]). The lens in front of D_1 is then needed to transfer the modulation back to coordinate space for imaging.

8. CONCLUSIONS

In conclusion, we have proposed a new type of two-object ghost imaging apparatus that cancels phase effects from thin objects in the vicinity of a particular plane and that allows comparisons between pairs of objects. The method involves a relatively simple apparatus and can be done with either entangled photon pairs or with a classically correlated light source. This apparatus may have potential for new applications in biomedical research, industry, and other fields.

ACKNOWLEDGMENTS

This work was supported by a U. S. Army Research Office (USARO) Multidisciplinary University Research Initiative (MURI) grant; by the Bernard M. Gordon Center for Subsurface Sensing and Imaging Systems (CenSSIS), a National Science Foundation (NSF) engineering research center; by the Defense Advanced Research Projects Agency (DARPA) InPho program; and by the Intelligence Advanced Research Projects Activity (IARPA) via USARO through grant W911NF-07-1-0629.

REFERENCES

1. T. B. Pittman, Y. H. Shih, D. V. Strekalov, and A. V. Sergienko, "Optical imaging by means of two-photon quantum entanglement," Phys. Rev. A **52**, R3429–R3432 (1995).
2. R. S. Bennink, S. J. Bentley, and R. W. Boyd, "Two-photon coincidence imaging with a classical source," Phys. Rev. Lett. **89**, 113601 (2002).
3. R. S. Bennink, S. J. Bentley, R. W. Boyd, and J. C. Howell, "Quantum and classical coincidence imaging," Phys. Rev. Lett. **92**, 033601 (2004).
4. A. Gatti, E. Brambilla, M. Bache, and L. A. Lugiato, "Correlated imaging, quantum and classical," Phys. Rev. A **70**, 013802 (2004).
5. Y. J. Cai and S. Y. Zhu, "Ghost imaging with incoherent and partially coherent light radiation," Phys. Rev. E **71**, 056607 (2005).

6. A. Valencia, G. Scarcelli, M. D'Angelo, and Y. H. Shih, "Two-photon imaging with thermal light," Phys. Rev. Lett. **94**, 063601 (2005).
7. G. Scarcelli, V. Berardi, and Y. H. Shih, "Can two-photon correlation of chaotic light be considered as correlation of intensity fluctuations?," Phys. Rev. Lett. **96**, 063602 (2006).
8. F. Ferri, D. Magatti, A. Gatti, M. Bache, E. Brambilla, and L. A. Lugiato, "High-resolution ghost image and ghost diffraction experiments with thermal light," Phys. Rev. Lett. **94**, 183602 (2005).
9. D. Zhang, "Correlated two-photon imaging with true thermal light," Opt. Lett. **30**, 2354–2356 (2005).
10. J. D. Franson, "Nonlocal cancellation of dispersion," Phys. Rev. A **45**, 3126–3132 (1992).
11. A. M. Steinberg, P. G. Kwiat, and R. Y. Chiao, "Dispersion cancellation in a measurement of the single-photon propagation velocity in glass," Phys. Rev. Lett. **68**, 2421–2424 (1992).
12. O. Minaeva, C. Bonato, B. E. A. Saleh, D. S. Simon, and A. V. Sergienko, "Odd- and even-order dispersion cancellation in quantum interferometry," Phys. Rev. Lett. **102**, 100504 (2009).
13. C. Bonato, A. V. Sergienko, B. E. A. Saleh, S. Bonora, and P. Villoresi, "Even-order aberration cancellation in quantum interferometry," Phys. Rev. Lett. **101**, 233603 (2008).
14. C. Bonato, D. S. Simon, P. Villoresi, and A. V. Sergienko, "Multiparameter entangled-state engineering using adaptive optics," Phys. Rev. A **79**, 062304 (2009).
15. D. S. Simon and A. V. Sergienko, "Spatial-dispersion cancellation in quantum interferometry," Phys. Rev. A **80**, 053813 (2009).
16. L. M. Jawerth, S. Münster, D. A. Vader, B. Fabry, and D. A. Weitz, "A blind spot in confocal reflection microscopy," Biophys. J. **98**, L01–L03 (2010).
17. J. A. Pedersen and M. A. Swartz, "Mechanobiology in the third dimension," Ann. Biomed. Eng. **33**, 1469–1490 (2005).
18. P. Friedl and K. Wolf, "Tumour-cell invasion and migration: diversity and escape mechanism," Nat. Rev. Cancer **3**, 362–374 (2003).
19. P. Friedl, K. Maaser, C. E. Klein, B. Niggemann, G. Krohne, and K. S. Zänker, "Migration of highly invasive MV3 melanoma cells in collagen lattices causes local matrix reorganization of $\alpha 2$ and $\beta 1$ integrins and CD44," Cancer Res. **57**, 2061–2070 (1997).
20. J. E. Landegent, N. Jansen in de Wal, G.-J. B. van Omment, F. Baas, J. J. M. de Vijlderi, P. van Duijn, and M. van der Ploeg, "Chromosomal localization of a unique gene by non-autoradiographic *in situ* hybridization," Nature **317**, 175–177 (1985).
21. J. E. Landegent, N. Jansen in de Wal, and J. S. Ploem, M. van der Ploeg, "Sensitive detection of hybridocytochemical results by means of reflection-contrast microscopy," J. Histochem. Cytochem. **33**, 1241–1246 (1985).
22. K.-H. Jeong, J. Kim, and L. P. Lee, "Biologically inspired artificial compound eyes," Science **312**, 557–561 (2006).
23. S. Mair, B. Gompf, and M. Dressel, "Microspectroscopy and imaging in the THz range using CW radiation," Phys. Med. Biol. **47**, 3719–3725 (2002).
24. E. Verhagen, A. L. Tchebotareva, and A. Polman, "Erbium luminescence imaging of infrared surface plasmon polaritons," Appl. Phys. Lett. **88**, 121121 (2006).
25. M. H. Rubin, D. N. Klyshko, Y. H. Shih, and A. V. Sergienko, "Theory of two-photon entanglement in type-II optical parametric down-conversion," Phys. Rev. A **50**, 5122–5133 (1994).